Magnetic Fiber Integrator and its Application in Precision Noninvasive DC Current Sensor

Ladislav Grno

***Abstract*— This paper is concerned with novel method of exact magnetic field sensing and line integration along path required for specific application. One of important applications is the electric current measurement. The sensor based on the presented method can be therefore used as precision dc current sensor. The realized openable flexible current probe based on the magnetic fiber integrator can cover current levels from fraction of A to tens of kA with negligible power and space requirements. Due to the true line integration, the measured current value is independent of areal distribution of the magnetic field, and therefore, the initial laboratory calibration is valid for field applications. The theory is experimentally validated with magnetic integrator for electrical current measurement, but it is not limited to this application only. The method is applicable in variety of instruments exploiting magnetic field evaluation.**

***Index Terms*— Current sensor, magnetic field measurement, magnetic saturation, magnetic sensors, magnetometer, power measurement.**

I. Introduction

MEASUREMENT of dc content of the electric current is an important task for control and monitoring used in industrial applications for example electrowinning, electrolysis, galvanic metallization, motor management, power supplies, welding supplies, and power line protection.

Comprehensive reviews of the state-of-the-art principles and realizations can be found in [1] and [2].

Most of the methods of noninvasive dc current measurement are based on evaluation of the magnetic field created by the electric current as a measure of this current. The sensors can exploit various principles, such as Hall effect, fluxgate, magnetoresistance, high frequency impedance, and nonlinearity. An overview of magnetic sensor problematics can be found in [3]. The main disadvantage of these principles is the principal nonlinear response depending on ambient conditions. Therefore, for precision applications, these sensors are used as null indicators for concentrated magnetic field. The magnetic field of the current carrying conductor is concentrated via magnetic circuit made from soft magnetic material into a gap containing a local magnetic field sensor. The accuracy is achieved via additional electronic feedback control compensating the primary flux with flux generated by secondary winding and this way keeping the effective flux level in the sensor gap zero. The compensating secondary current is than the scaled measure for the primary current.

Generally, all methods based on concentration of the magnetic field into local magnetic field sensor via passive magnetic core suffer from nonlinearity and finite permeability of the real core material. Minimization of the core influence is achieved via increasing the mass of the core and by flux compensation. This approach leads especially for high currents to space consuming solutions and remarkable power consumption.

Different principles based on a Neel effect ac–dc current sensor designed with second harmonic sensing are proposed in [4]. The method actually uses nonlinearity of the superparamagnetic properties of the core to generate and evaluate harmonic content of an excitation signal. Even large linearity range is stated, the measurement based on nonlinear behavior is principally sensitive to local distribution of magnetic field and temperature cannot be therefore exactly described.

Simple approach to high current industrial measurement is presented in [5] where the magnetic core nonlinearity is used to generate voltage response of excited magnetic core. The output voltage is influenced by the magnetic field of the measured current. Due to many influencing factors, the method is principally limited to monitoring applications only. An approach to measure the magnetic field integral with multiple local Hall sensor and estimation of the field distribution is presented in [6]. This method can be used in predictable fixed installations but not for universal field applications.

To the state of the art belong also the transducers based on fiber-optic sensing elements that use the magnetic field surrounding the conductor to modulate the condition of light propagation in optical path [7]. The advantages of these systems are the intrinsic safety associated with fiber-optic and rejection of ambient electromagnetic interference. The fiber-optic sensors are sensitive to environmental conditions that can alter the birefringence along the fiber, resulting to scale factor variation. Generally, the fiber-optic devices are very complex and therefore for ordinary applications expensive.

The presented fiber integrator method enables true integration of the magnetic field along flexible magnetic fiber without any additional magnetic circuits.

II. Magnetic Fiber Integrator Arrangement

The presented sensor [10] consists of a flexible fiber from soft magnetic material with negligible cross-sectional area compare to the length of the fiber. The fiber has uniform

Manuscript received June 6, 2016; revised February 02, 2017; accepted February 07, 2017. Date of publication March 14, 2017; date of current version July 12, 2017. The Associate Editor coordinating the review process was Dr. Edoardo Fiorucci. (*Corresponding author: Ladislav Grno.*)

The author is with Applied Precision Ltd., 83104 Bratislava, Slovakia (e-mail: grno@appliedp.com).

Color versions of one or more of the figures in this paper are available online at http://ieeexplore.ieee.org.

Digital Object Identifier 10.1109/TIM.2017.2674339

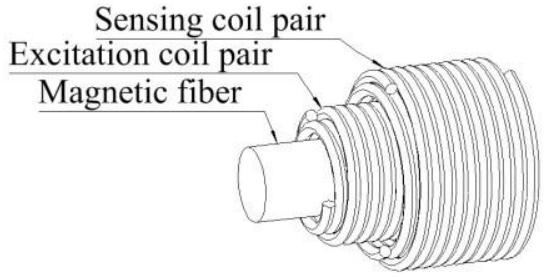

Fig. 1. Fiber winding arrangement.

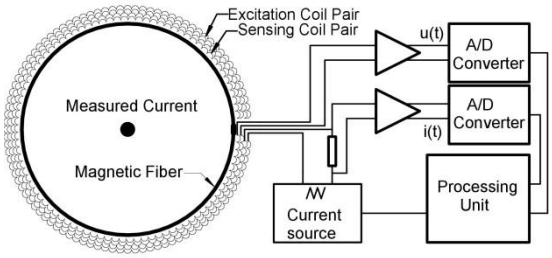

Fig. 2. Principal configuration of the fiber integrator.

cross-sectional area and uniform magnetic properties along the whole length. The fiber is equipped with excitation coil and with sensing coil. Both coils are wound on the fiber with uniform winding density along the whole length of the fiber. The principal sensor arrangement is shown in Fig. 1. The flexible fiber is equipped with excitation coil and sensing coil. The coils are wound as pair windings with members of the pair wound in mutually opposite direction. This arrangement enables interconnection of the winding pairs on one end of the coil and access to the whole coil on the opposite end.

The principal configuration of the fiber integrator with closed path around current carrying conductor is shown in Fig. 2.

In order to execute closed-loop integration which is required for the current measurement, the fiber ends are joined and this way the fiber equipped with the exciting and sensing coils creates a closed loop enclosing the conductor carrying the measured current. The current source generates the exciting current into the excitation coil. The excitation current is a triangle time function, which oscillates between two limiting values $\boldsymbol{I_1}$ and $\boldsymbol{I_2}$. First current limit is set to the value at which the exciting current, including the external magnetic field, excites the whole volume of the flexible fiber magnetic material into saturation state. The second current limit is set to value at which the exciting current, including the external magnetic field, excites the whole volume of the flexible fiber magnetic material into the opposite oriented saturation state.

The exciting current is passed through current shunt and signal conditioning circuit producing the current signal $\boldsymbol{i(t)}$. The sensing coil pair produces the induced voltage signal $\boldsymbol{u(t)}$.

The current signal $\boldsymbol{i(t)}$ and the voltage signal $\boldsymbol{u(t)}$ are fed into the processing unit which for one current slope calculates the definite integral of the time function of the product of the current signal and the voltage signal

$$\int_{T_1}^{T_2} i(t)u(t)dt$$

and the definite integral of the time function of the induced voltage

$$\int_{T_1}^{T_2} u(t)dt.$$

The integration time limits $\boldsymbol{T_1}$ and $\boldsymbol{T_2}$ correspond to the respective instant when calculation starts and finishes.

The same calculation is executed for opposite current slope with respective integration time limits $\boldsymbol{T_3}$ and $\boldsymbol{T_4}$.

The measured current is then calculated from the formula

$$I = W\left(\frac{\int_{T_1}^{T_2} i(t)u(t)dt}{\int_{T_1}^{T_2} u(t)dt} + \frac{\int_{T_3}^{T_4} i(t)u(t)dt}{\int_{T_3}^{T_4} u(t)dt}\right).$$

The cumulative conversion factor W includes the winding density of the excitation coil W_d, length of the sensor loop L, and conversion factor of the excitation current measuring circuit C_c.

The nominal value of the cumulative factor W can be calculated from the known parameters of the fiber sensor and evaluation circuitry

$$W = -0.5LW_dC_c$$

where

W_d winding density of the excitation coil;
L length of the sensor loop;
C_c conversion factor of the excitation current measuring circuit.

The exact value of conversion factor W can be obtained via calibration of individual sensor with measured reference current.

III. Magnetic Fiber Integrator Theory

The negligible cross-sectional area of the fiber suppresses the interaction of the neighboring fiber elements due to the magnetic flux continuity law and has negligible influence on the surrounding magnetic field strength. Therefore, the analysis of the whole sensor can be reduced to integration of partial contributions of the local elementary magnetic dipoles.

The magnetization of a local elementary magnetic dipole of the fiber and the corresponding signals in the time domain are shown in Fig. 3: the local external magnetic field intensity $\boldsymbol{H_e}$ is excited by the measured current and possible external sources. The internal magnetic field intensity $\boldsymbol{H_i}$ is excited by the excitation current injected into the excitation coil. The excitation current rises from the first limiting value $\boldsymbol{I_1}$ at time $\boldsymbol{T_1}$ toward the second current limiting value $\boldsymbol{I_2}$. Reaching the value $\boldsymbol{I_2}$ in time $\boldsymbol{T_2}$, the sign of the slope is changed so the current is returning to the starting value $\boldsymbol{I_1}$. The time interval for the return period is from $\boldsymbol{T_3}$ to $\boldsymbol{T_4}$. This process can be periodically repeated. The internal excitation magnetic field created by the excitation current is added to the external field and creates the effective field $\boldsymbol{H_s}$ magnetizing the

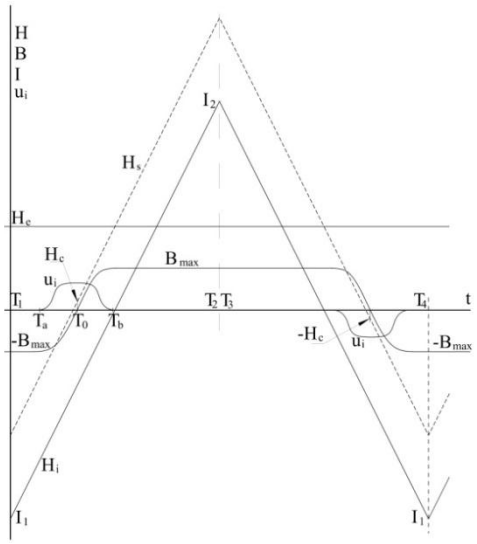

Fig. 3. Magnetization of local elementary magnetic dipole as function of time.

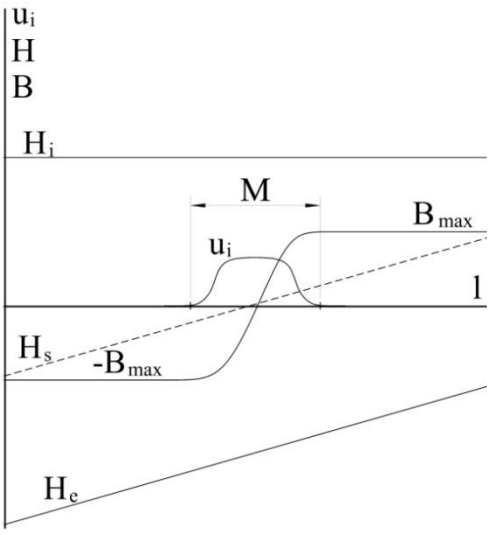

Fig. 4. Example of momentary magnetization along the fiber length.

magnetic material of the fiber. The magnetic flux within the fiber material corresponds to the effective field H_s according to the magnetization function of the fiber material. The magnetization function has an offset equal to coercive force H_c. The sign of the offset depends in the direction of the current slope. The transition from the saturated value $B_{\max}$ through the active nonsaturated region of the magnetization function generates local induced voltage u_i with momentary value depending on the derivation of the magnetization function, cross-sectional area of the fiber and winding density. The locally induced voltage into the homogeneous coil winding linearly contributes to the total voltage induced into the coil along the whole fiber length.

The magnetic field of the local dipole generally interacts with neighboring dipoles due to magnetic flux continuity law. The interaction length depends on the relative permeability of the fiber material. The higher the relative permeability of the fiber the longer is the interaction length. In case of very low relative permeability, the magnetic flux leaks from the fiber and the field diminish with increasing distance from the local magnetic field source. A different situation occurs if the relative permeability is extremely high. In this case, the fiber tends to homogenize the magnetic flux by squeeze of the field intensity into less magnetized fiber localities. The mutual interaction of the sensor fiber with external magnetic field affects theoretically the external magnetic field intensity distribution compare to distribution of the surrounding magnetic field intensity without the fiber but due to negligible volume of the fiber this effect can be neglected. The magnetic flux distribution along the fiber depends on the distribution of the external magnetic field. For an ideal constant magnetic field distribution which exists on circle around round conductor with homogeneous coaxial return path without presence of any external field, the whole fiber material is magnetized simultaneously and generates the induced voltage corresponding to change of magnetization state of the whole volume of the fiber material at the same time. In real situation, the external magnetic field intensity is position dependent, and therefore, the local value of induced voltage density along the fiber depends on the current carrying conductor arrangement, the external field sources, and the shape of the fiber loop geometry.

An example of effect of linearly increasing external magnetic field intensity on the magnetization of the fiber is shown in Fig. 4. The figure shows a time sample of longitudinal distribution of fiber magnetization and induced voltage density at the same time instant.

In this example, the value of external magnetic field intensity $\boldsymbol{H_e}$ is increasing along the fiber section. The internal magnetic field intensity $\boldsymbol{H_i}$ is uniform along the whole fiber length due to uniform excitation coil winding density. The magnetic flux in the fiber material responds the effective field $\boldsymbol{H_s}$ according to the magnetization function. The transition from the saturated value $\boldsymbol{B_{max}}$ through the active nonsaturated region of the magnetization function causes position-dependent value of the locally generated induced voltage density $\boldsymbol{u_i}$. The active nonsaturated region $\boldsymbol{M}$ along the fiber contributes to the cumulative value of the induced voltage appearing on the sensing coil terminals. Due to uniform winding density of the sensing coil along the fiber, the induced voltage is equal to the line integral of the local induced voltage $\oint \boldsymbol{u_i(l,t)dl}$ along the whole fiber. The internal magnetic field intensity $\boldsymbol{H_i}$ is time dependent due to variable excitation. Therefore, the position of the active nonsaturated region $\boldsymbol{M}$ travels along the fiber respective to effective field intensity. The width of the active region depends on the gradient of the external field along the fiber. Lower gradient yields wider active region and vice versa. Limit state is the uniform external field along the fiber which yields simultaneous excitation of the whole fiber. For example, such uniform field is excited inside toroidal coil along circle concentric with axe of the toroid.

The local magnetic flux density $\boldsymbol{B}$ in the fiber depends on the magnetization function of the magnetic material of the

fiber. Generally, the magnetization function (B–H function) of ferromagnetic material includes hysteresis and therefore the magnetization depends on the history of the excitation. If the excitation is continuously increased or decreased and starts in one saturated region and ends in the other saturated region, then the magnetization function can be described by two identical but shifted functions. The magnetic field intensity exciting the long sensor fiber is generally position dependent. The local magnetic flux density $B(l)$ at longitudinal position $\boldsymbol{l}$ of the fiber is given by equations

$$B(l) = f((H_s(l)) - H_c) \tag{1}$$

$$B(l) = f((H_s(l)) + H_c) \tag{2}$$

where

f	magnetization function of the fiber;
$H_s(l)$	local effective magnetic field intensity at position l;
H_c	coercive force of the fiber magnetic material.

The functions (1) or (2) are valid for continuously increasing or continuously decreasing magnetic field intensity starting in saturated region.

The exciting current flowing through the homogeneous winding with uniform density along the fiber creates uniform internal exciting magnetic field inside the fiber. The field is oriented in the direction of the fiber axe with intensity $\boldsymbol{H_i}$. The effective magnetic field intensity $\boldsymbol{H_s}$ exciting the fiber is the sum of internal magnetic field intensity and position-dependent external magnetic field intensity

$$H_s(l) = H_e(l) + H_i \tag{3}$$

where $H_e(l)$ is the external magnetic field intensity at position l and H_i is the internal uniform magnetic field intensity created by the exciting current.

The local induced voltage density, i.e., voltage per length unit in the sensing winding at local position l is according to Faraday's law given by equation

$$u_i(l) = K\frac{d\boldsymbol{B}(\boldsymbol{l})}{dt} = Kf'(H_s(l)) \tag{4}$$

where

$u_i(l)$	induced voltage density at position l;
$B(l)$	magnetic flux at local position l;
K	factor comprising cross-sectional area of the fiber, winding density and direction.

Change of exciting current with constant slope yields for the internal magnetic field intensity a linear time function

$$H_i(t) = h_0 + h_1 t. \tag{5}$$

Equation (4) for positive current slope yields

$$u_i(l,t) = Kf'(H_e(l) + h_0 + h_1 t - H_c). \tag{6}$$

Continuous multiplication of instant values of internal exciting magnetic field intensity and induced voltage yields their product as function of time

$$Q(l,t) = H_i(t)u_i(l,t). \tag{7}$$

Integration of the product $Q(l,t)$ as the function of time in the interval $[T_1,\ T_2]$ yields for the local definite integral at position l the equation

$$\int_{T_1}^{T_2} Q(l,t)dt = K\int_{T_1}^{T_2}((h_0 + h_1 t)f'(H_e(l) + h_0 + h_1 t - H_c))dt. \tag{8}$$

The definite integral in the time interval $[T_1,\ T_2]$ can be arranged as the sum of definite integrals in three time intervals

$$\int_{T_1}^{T_2} Q(l,t)dt = \int_{T_1}^{T_a} Q(l,t)dt + \int_{T_a}^{T_b} Q(l,t)dt + \int_{T_b}^{T_2} Q(l,t)dt. \tag{9}$$

At the time T_1, the effective magnetic field intensity H_s starts in first saturated region. At the time T_a, H_s leaves the saturated region and enters the active magnetization region of the fiber material, and at the time T_b, H_s leaves the active magnetization and enters the second saturated region. At the time T_2, the excitation ends in the second saturated region.

The value of relative permeability directly determines the value of derivation f' of the magnetization function. The contribution of the saturated regions to the integral (9) compare to the contribution of the active magnetization region is negligible due to high permeability of the mumetal fiber with the typical relative permeability of 80 000–100 000. Equation (9) can be therefore simplified to

$$\int_{T_1}^{T_2} Q(l,t)dt = \int_{T_a}^{T_b} Q(l,t)dt. \tag{10}$$

For continuously increasing excitation current, i.e., positive slope, considering time as input variable according to (5), the magnetization function is an even function centered about the excitation time T_0 when the magnetic flux density $B(l,0)$ equals zero

$$f(H_e(l) + h_0 + h_1 T_0 - H_c) = 0. \tag{11}$$

Due to symmetry, T_0 is the center of the time interval $[T_a,\ T_b]$

$$T_0 = (T_a + T_b)/2; \quad \Delta T = (T_b - T_a)/2. \tag{12}$$

Formal transformation of the time axis via shifting the origin to T_0 yields

$$f(H_e(l) + H_i(l,T_0) - H_c) = 0. \tag{13}$$

The definite integral (9) with application of (12) and (13) can be rewritten as

$$\int_{T_a}^{T_b} Q(l,t)dt = \int_{-\Delta T}^{\Delta T}(H_i(l,T_0) + h_1 x)f'(h_1 x)dx \tag{14}$$

where x is the transformed time variable

$$x = t - T_0. \tag{15}$$

Rearranging (14), we get

$$\int_{T_a}^{T_b} Q(l,t)dt = K\left[\int_{-\Delta T}^{\Delta T} H_i(l,0)f'(h_1x)dx + \int_{-\Delta T}^{\Delta T} h_1xf'(h_1x)dx\right]. \quad (16)$$

The function $Kh_1xf'(h_1x)$ is proportional to the product of odd function h_1x and even function $f'(h_1x)$ and therefore odd function. The definite integral of the odd function with symmetrical limits $\pm\Delta T$ is zero

$$\int_{-\Delta T}^{\Delta T} h_1xf'(h_1x)dx = 0. \quad (17)$$

The definite integral (16) can be therefore rewritten as

$$\int_{T_1}^{T_2} Q(l,t)dt = KH_i(l,0)\int_{-\Delta T}^{\Delta T} f'(h_1x)dx. \quad (18)$$

After integration considering (10) and (11), we have

$$\int_{T_1}^{T_2} Q(l,t)dt = 2KB_{\max}(H_c - H_e(l)) \quad (19)$$

where $B_{\max}$ is the saturated magnetic flux density of the fiber material.

Having uniform magnetic properties, uniform cross-sectional area, and uniform winding density along the whole fiber length, the sum of local contributions of the fiber along the whole closed circle can be written as a closed line integral from 0 to the whole fiber length L

$$\oint_0^L \int_{T_1}^{T_2} Q(l,t)dtdl = 2KB_{\max}\left(LH_c - \oint_0^L H_e(l)dl\right). \quad (20)$$

Due to mutual independence of the time function and the position function in the double integral $\oint_0^L \int_{T_1}^{T_2}$ the integration sequence on the left-hand side of (20) can be rearranged

$$\begin{aligned}\oint_0^L \int_{T_1}^{T_2} Q(l,t)dtdl &= \int_{T_1}^{T_2} \oint_0^L Q(l,t)dldt \\ &= \int_{T_1}^{T_2} LH_i(t) \oint_0^L u_i(l,t)dldt \\ &= \int_{T_1}^{T_2} LH_i(t)u(t)dt \end{aligned} \quad (21)$$

where $u(t)$ is the momentary induced voltage at time t appearing on the whole sensing coil, i.e., integrated along the whole fiber length.

Rewriting the equation (20) using (21), we get

$$\int_{T_1}^{T_2} LH_i(t)u(t)dt = 2KB_{\max}\left(LH_c - \oint_0^L H_e(l)dl\right). \quad (22)$$

The closed line integral of the external magnetic field intensity $\oint_0^L H_e(l)dl$ corresponds according to Ampere's law exactly to the current enclosed by the fiber loop. Equation (22) then yields for the measured current enclosed by the fiber loop the equation

$$I = \oint_0^L H_e(l)dl = LH_c - \frac{L\int_{T_1}^{T_2} H_i(t)u(t)dt}{2K*B_{\max}}. \quad (23)$$

The factor $2KB_{\max}$ can be calculated via integration of the induced coil voltage

$$\begin{aligned}\oint_0^L \int_{T_1}^{T_2} u_i(l,t)dtdl &= \int_{T_1}^{T_2} \oint_0^L u_i(l,t)dldt \\ &= \int_{T_1}^{T_2} u(t)dt = 2KB_{\max} \end{aligned} \quad (24)$$

yielding the equation

$$2KB_{\max} = \int_{T_1}^{T_2} u(t)dt. \quad (25)$$

Implementing (25) into (23), we get

$$I = LH_c - \frac{L\int_{T_1}^{T_2} H_i(t)u(t)dt}{\int_{T_1}^{T_2} u(t)dt}. \quad (26)$$

The same evaluation procedure for excitation current with negative slope

$$H_i(t) = h_0 - h_1t \quad (27)$$

in the time interval $[T_3, T_4]$ yields

$$I = -LH_c - \frac{L\int_{T_3}^{T_4} H_i(t)u(t)dt}{\int_{T_3}^{T_4} u(t)dt}. \quad (28)$$

The sum of (26) and (28) eliminates the coercive force H_c and yields the equation for measured current

$$I = -0.5L\left(\frac{\int_{T_1}^{T_2} H_i(t)u(t)dt}{\int_{T_1}^{T_2} u(t)dt} + \frac{\int_{T_3}^{T_4} H_i(t)u(t)dt}{\int_{T_3}^{T_4} u(t)dt}\right). \quad (29)$$

The internal magnetic field intensity $H_i(t)$ can be calculated from the excitation current, the winding density and current signal conversion factor (shunt resistance and amplifier gain)

$$H_i(t) = i(t)W_dC_c \quad (30)$$

where

$i(t)$ excitation current;
W_d excitation winding density;
C_c current signal conversion factor.

Application of (30) into (29) yields the final measurement equation

$$I = W\left(\frac{\int_{T_1}^{T_2} i(t)u(t)dt}{\int_{T_1}^{T_2} u(t)dt} + \frac{\int_{T_3}^{T_4} i(t)u(t)dt}{\int_{T_3}^{T_4} u(t)dt}\right) \quad (31)$$

where

$$W = -0.5LW_dC_c \quad (32)$$

is the cumulative sensor conversion constant.

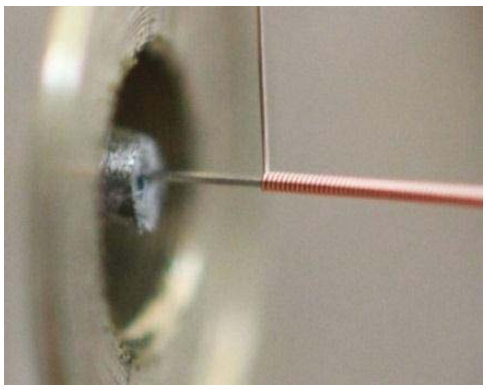

Fig. 5. Detail of winding of 50-μm copper wire on 125-μm mumetal fiber.

IV. Sensor Embodiment

The presented method has been verified on the realized sensor based on 125-μm-diameter continuous mumetal fiber equipped with six-layer 50-μm copper wire exciting coil and two-layer 50-μm copper wire sensing coil. The layers are continuously wound with altered winding direction creating forward and return winding pairs. We have developed special winding machine with processor control of the winding density. Macrophotography of the first layer winding process is shown in Fig. 5.

The equally directed layers of the excitation coil windings are parallelized in order to minimize the resistance, i.e., the power needed for excitation. The layers with the opposite direction create respective forward and return path for the excitation current. The sensing coil has the same mutually opposite winding arrangement. The outer diameter of the finalized sensor fiber setup is approximately 1 mm. The resistance of the exciting coil is approximately 120 Ω/m.

The maximum current into the exiting coil is limited by the maximum power dissipation keeping the sensor temperature rise at acceptable level. The above-described construction is without any additional cooling capable to dissipate approximately 10 W per 1-m sensor length. Due to sawtooth current time function, the effective power is significantly less than the peak power. The maximum peak excitation current of 0.4 A was found as continuously applicable. The winding density 36 000 turns/m (18 000 forward and 18 000 return) yields the maximum exciting magnetic field intensity of 14.4 kA/m.

Generally, for real measurement, an appropriate reserve must be left cover the maximum possible local field intensity. The magnetic field distribution is for practical field application not fully predictable, and therefore, the maximum excitation must be dimensioned for the maximum local field. Fortunately, the fully saturated end state of the entire magnetic fiber, which is the basic condition for the correct measurement, can be monitored via value of the induced voltage integral (25). If the saturation state in the entire volume of the fiber is fully reversed, the value of the voltage integral is constant. Decreased value of the voltage integral (25) indicates local overload, i.e., local magnetic field level which cannot be overridden by the exciting current.

The maximum allowed excitation current is determined by maximum effective dissipated power. Therefore, with less dense sampling, i.e., delays between opposite current slope pairs, the maximum excitation current can be increased inversely to the decreased effective dissipated power mean value.

Further increase of the maximum current can be achieved via removal of the dissipated heat via appropriate cooling system.

V. Evaluation Unit

The evaluation unit integrates all control, sampling, and data processing components, including the variable current source and current transducer circuit. The evaluation unit is additionally equipped with voltage input for optional power and energy measurement. The current and voltage signals from the dc sensor, the voltage input, and the ac sensor are sampled with synchronous 24-bit Delta–Sigma Analog-to-digital converter (ADC) (ADS1274) configured for 100-kHz sampling rate.

The 24-b ADC with a specified maximum nonlinearity of 12 ppm and a temperature drift of 1.3 ppm/°C, voltage reference REF5025 with maximum temperature drift 3 ppm/°C along with the precision current shunt of 10 ppm/°C and precision signal conditioning amplifier suppress the influence of the evaluation unit on the measurement under 0.01% in the temperature range 25 °C ± 10 °C.

The control of the system, current source, data processing, and real-time calculation of measurement result is executed by dual-core LPC4330 cortex-M4/M0 microcontroller.

The whole evaluation unit is cased into 88-mm-wide DIN rail mounting box with Liquid crystal display graphic display. The remote control of the unit inclusive data exchange is accomplished via RS-485 communication port. The measured current is available on analog output as well.

VI. Measurement Error Sources

The basic conditions for measurement accuracy are uniformity of the magnetic fiber cross section and the winding density along the sensor. These basic conditions ensure correct integration of the magnetic field independent of the field distribution. These basic conditions are limited by the technologies available for magnetic fiber production and winding process.

Equation (31) is valid for the closed loop. The real fiber sensor cannot be exactly closed due to unavoidable mechanical elements at the joined ends. The magnetic field present in the discontinuity gap is not included into the loop integral, and therefore, this residual gap creates unpredictable measurement error depending on the actual magnetic field distribution. This causes influence of the position of the current caring conductor inside the sensor and sensitivity to magnetic field with external origin.

One possibility of elimination of the gap impact is an additional sensing coil at the sensor end. The additional sensing coil extrapolates the end condition of the fiber into the gap.

Another elimination of the gap impact possibility is the application of high permeability magnetic material around the junction. The magnetic material squeezes the magnetic field

from the gap region into the homogeneous and thus accurate sensor region. The effect of the magnetic material can be explained as a magnetic short circuit across the gap. The local redistribution of the magnetic field has no effect on the function of the sensor due to Ampere's law $\oint H \cdot dl = I$ independence from the magnetic field distribution along the integrating path.

The premise for the presented theory is the alternation of opposite fully saturated states of the fiber magnetic material. The magnetization function of real magnetic material differs from idealized function with constant magnetic induction $B_{\max}$ in the saturated state. The magnetic induction in real material continuously increases even in the quasi-saturated state. This nonlinear magnetization in the quasi-saturated state causes deviation from the mathematical model when the measured field intensity is close to maximum field intensity excited by the maximum excitation current. This deviation causes linearity error for measured external field approaching the excitation end value. This end effect can be in some extent predicted from the measured current value, and therefore, the calibration model can be modified to reduce this effect.

VII. Sensor Evaluation Setup

The presented sensor is inserted into SymmProFlex Rogowski ac probe [8], [9]. The prefabricated shielded cable is based on Polytetrafluoroethylene tubes shielded with mutually opposite wound groups of enameled wires interconnected only in one place at the end of the cable. The outer diameter of the cable over insulation is 6 mm. The insulation is designed to withstand 6-kV test voltage. The principal advantage of this patented shielding arrangement is its maximum flexibility at maximum noninductive coverage, but unlike standard bare wire shielding, the enameled wire shield does not enable induction of transversal current in transversal plane the shielding.

The measured dc content and ac content are summed and this way creates the recovered original signal.

Arrangement of the dc and ac sensor fibers in the probe cable is shown in Fig. 6.

The functionality and accuracy of the dc part and respective electronics of the complex ac /dc probe was evaluated with 200A precision dc current source. The reference for the source is the voltage output of FLUKE 5700-A multifunction calibrator. The dc current source feeds 56 turn toroid and this way generates up to 11.2 kA of equivalent dc current and respective homogeneous magnetic field.

Generation of local field for testing of correct integration along the whole sensor exposed to nonhomogeneous magnetic field is realized via 1.2-m-diameter coil with 6 turns of 25 mm^2 cross-sectional wire. The high current source setup is shown in Fig. 7.

VIII. Test Results

The function of the sensor is based on integration of local magnetic field along the sensor fiber. The distribution of the magnetic field can be easily monitored via induced voltage

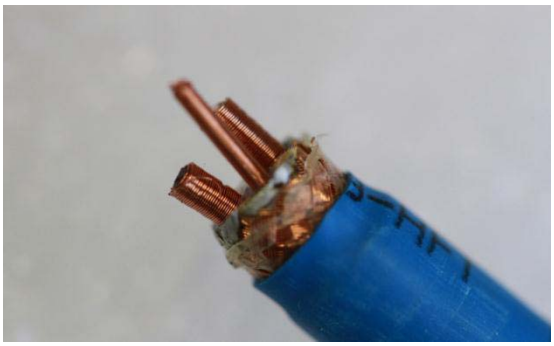

Fig. 6. Arrangement of the dc and ac sensor fibers in the probe cable.

Fig. 7. High current source setup.

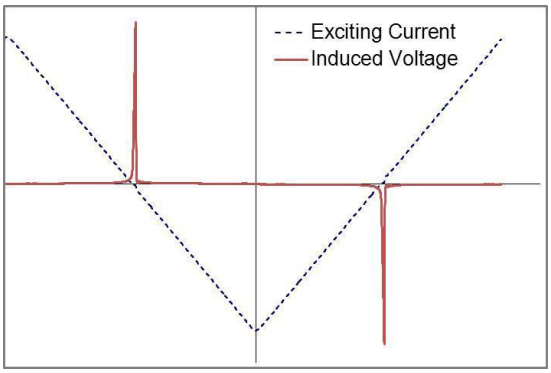

Fig. 8. Waveform of exciting current and induced voltage response at zero test current.

generated on the sensing coil as function of time, i.e., related to the exciting current.

The waveform of exciting current and induced voltage response at zero test current is shown in Fig. 8.

The narrow peaks show the simultaneous exchange of the magnetization state of the whole fiber around the zero excitation current.

The induced voltage response of the sensor placed into calibration toroid with 5600-A effective current approaching the maximum excitation current is shown in Fig. 9. The larger spread of the voltage response compare to the zero current state indicates variable magnetic field along the fiber due to nonideal winding homogeneity of the exciting toroid coil.

Shift of the center of the magnetization function of the fiber toward maximum excitation current decreases the end values of the fiber magnetization. This effect can be seen as decreasing value of integral (25) toward high current values. The decreasing integral value in percentage related to the maximum value at zero current is shown in Fig. 10. This end

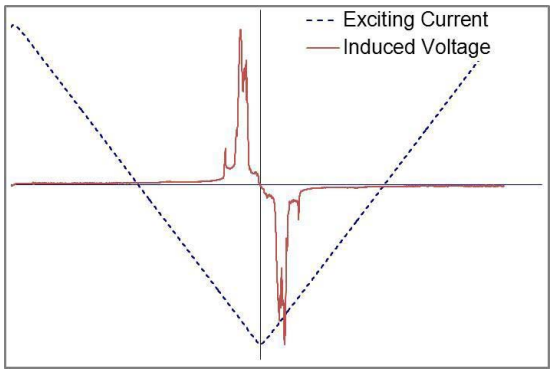

Fig. 9. Waveform of exciting current and induced voltage response at 5600-A test current.

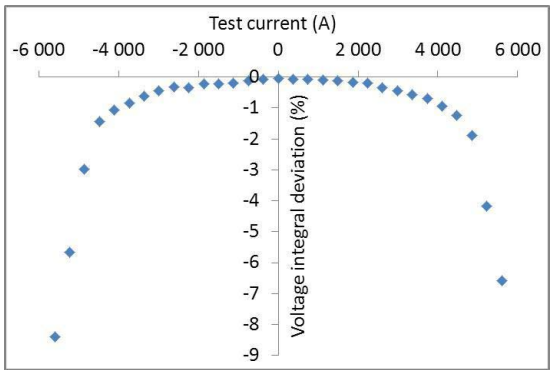

Fig. 10. Decrease of voltage integral with increasing current.

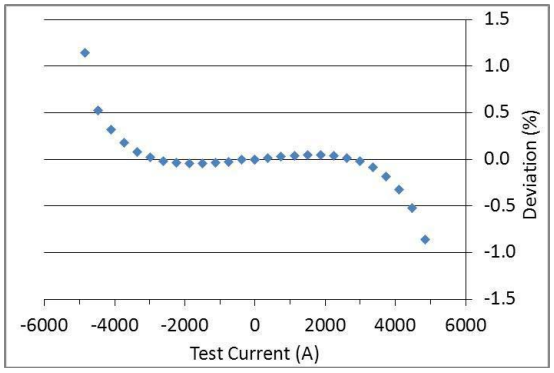

Fig. 11. Measured deviations from linear calibration model.

effect affects the linearity of the transfer function when the measured current approaches the maximum excitation current.

The linear fit data response of the 500-mm-long dc sensor with 400-mA peak exciting current calculated from formula (31) in range of -5600 to $+5600$ A is shown in Fig. 11.

The percentage differences are relative to 5600-A end value. The deviation from the linear trend line toward the range end is caused by the decrease of the fiber magnetization approaching the maximum excitation current.

The difference of the measured value from the calibration model including end effect compensation related to 5600-A end value is shown in Fig. 12.

The maximum resolution of the sensor has been tested with ± 20 mA peak value excitation current. This excitation current

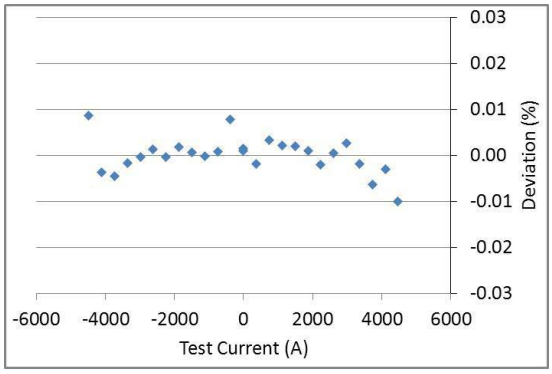

Fig. 12. Measurement with calibration model including the end effect compensation.

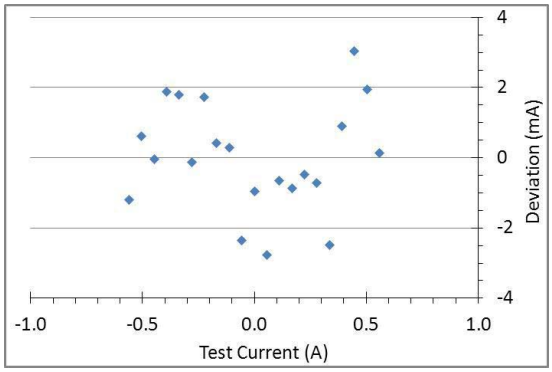

Fig. 13. Low current deviations from linear calibration model.

corresponds to approximately 300-A maximum current. The noise represented as deviation of measured current from the test current in range ± 0.8 A with linear calibration model is shown in Fig. 13.

The observed deviations can be interpreted as random noise spread within ± 3 mA peak values with a standard deviation of 1.5 mA. This current corresponds in the 0.5-m circumference length of the sensor to 3-mA/m magnetic field intensity and thus corresponding to magnetic induction 2.4 nT. This low noise behavior enables to use the presented method for wide range of magnetic applications. For example, the opened probe formed into straight line proved to be an excellent vector sensor of earth magnetic field.

The position sensitivity of the realized sensor has been tested with a local current of 600 A at various positions of probe located directly on the test current carrying conductor (six-wire bundle) at positions from 1 h to 12 h. The probe located at 12 h which corresponds to the position of the sensing fiber junction is shown in Fig. 14.

The induced voltage response shown in Fig. 15 demonstrates the typical field distribution for local excitation, i.e., sensor located directly on the test current carrying conductor. The main peak of induced voltage near zero excitation current indicates that the most of the fiber material is exposed to low external field. The local peak at higher excitation level indicates the local magnetic field concentration created by the nearby conductor.

Fig. 14. Arrangement for position influence measurement.

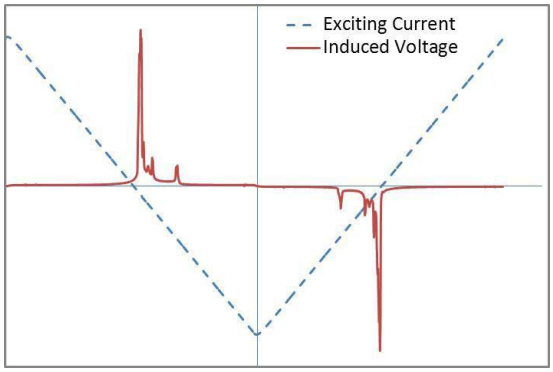

Fig. 15. Waveform of exciting current and induced voltage response at local excitation.

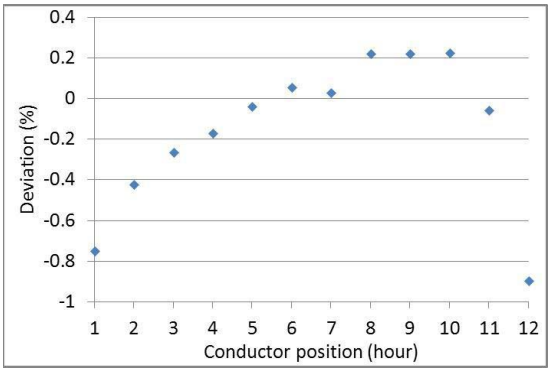

Fig. 16. Local sensitivity deviations without junction gap compensation.

The result of measurement of local sensitivity along the sensor cable without any junction gap compensation is shown in Fig. 16.

Simple magnetic screening made from single layer 0.3-mm-thick soft magnetic iron tape ring placed around the probe junction as shown in Fig. 17 resulted to significant reduction of local deviations as shown in Fig. 18.

Increasing the probe distance from the current caring conductor significantly decreases the position depending deviation from the calibration value. In the center of the probe, the measured value corresponds to the calibration data obtained from the toroidal calibration system.

The environmental influence and stability of the probe has been tested via response to thermal cycling. We have tested the probe located in thermal chamber generating temperature variations between −20 °C and 60 °C. The measured deviation from the initial calibration value at 23 °C is shown in Fig. 19.

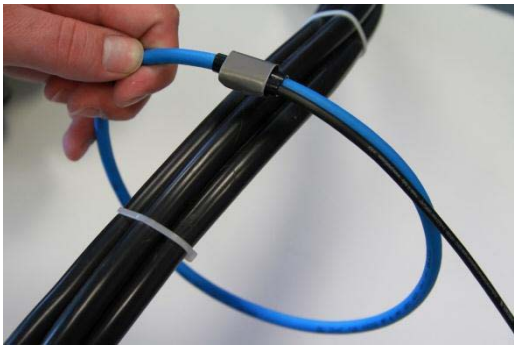

Fig. 17. Magnetic screening ring around the probe junction.

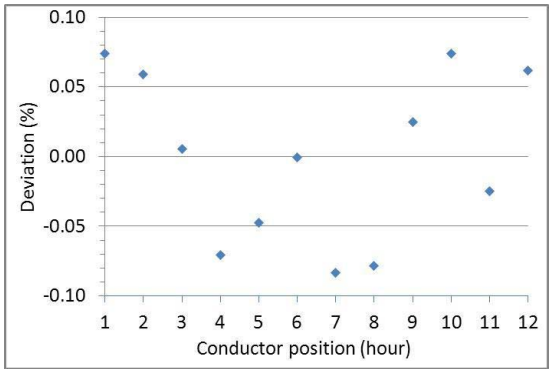

Fig. 18. Local sensitivity deviations with magnetic screening.

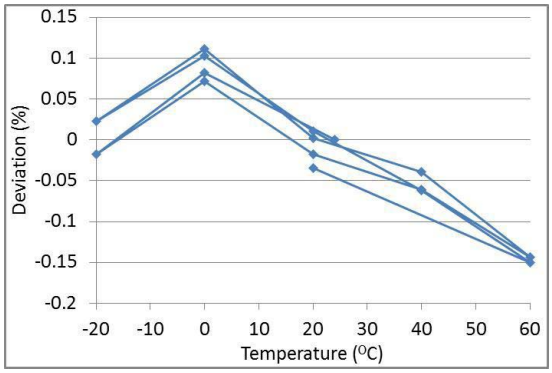

Fig. 19. Relative deviation of probe response to temperature cycling.

The maximum deviation in the range of −20 °C to 60 °C is approximately 0.25%. The TC in the range of 0 °C–60 °C is better than 50 ppm/K. The observed hysteresis ±0.03% is originated in slow temperature gradient decay within the probe body compared to the 30-min. sampling interval.

IX. Conclusion

The presented magnetic field integration method can significantly improve the state of the art in magnetic field evaluation and especially in noninvasive dc current measurement. The laboratory test results on magnetic fiber-based dc current probe for ac / dc power and energy meter verified the correctness of the presented theory and showed its potential for laboratory and industrial applications. The presented integration method is experimentally validated on the fiber integrator, but,

principally, it is applicable in various different macroscopic or microscopic magnetic circuits as well.

REFERENCES

[1] S. Ziegler, R. C. Woodward, H. H.-C. Iu, and L. J. Borle, "Current sensing techniques: A review," *IEEE Sensors J.*, vol. 9, no. 4, pp. 354–376, Apr. 2009.

[2] P. Ripka, "Electric current sensors: A review," *Meas. Sci. Technol.*, vol. 21, no. 11, p. 112001, 2010.

[3] P. Ripka and M. Janosek, "Advances in magnetic field sensors," *IEEE Sens. J.*, vol. 10, no. 6, pp. 1108–1116, Jun. 2010.

[4] E. Vourc'h, Y. Wang, P.-Y. Joubert, B. Revol, A. Couderette, and L. Cima, "Neel effect toroidal current sensor," *IEEE Trans. Magn.*, vol. 49, no. 1, pp. 81–84, Jan. 2013.

[5] E. Fiorucci and G. Bucci, "A low-cost contactless transducer for the measurement of DC currents up to 13 kA for the industry of anodized aluminum," *IEEE Trans. Instrum. Meas.*, vol. 62, no. 4, pp. 845–852, Apr. 2013.

[6] J. Y. C. Chan, N. C. F. Tse, and L. L. Lai, "A coreless electric current sensor with circular conductor positioning calibration," *IEEE Trans. Instrum. Meas.*, vol. 62, no. 11, pp. 2922–2928, Nov. 2013.

[7] R. M. Silva *et al.*, "Optical current sensors for high power systems: A review," *Appl. Sci.*, vol. 2, no. 3, pp. 602–628, 2012, doi: 10.3390/app2030602.

[8] L. Grno, "Precision flexible current sensor," U.S. Patent 7 847 543 B2, Dec. 7, 2010.

[9] L. Grno, "Precision flexible current sensor," European Patent 1 960 796, Aug. 27, 2008.

[10] L. Grno, "Sensor and method for electric current measurement," European patent WO 2015/122 855, Aug. 8, 2015.

Ladislav Grno received the Dipl. Eng. degree in electrical engineering and the PhD. degree in measurement technique from Slovak Technical University, Bratislava, Slovakia, in 1971 and 1977, respectively.

He was with the Slovak Metrological Institute, Bratislava, where he was the Director of the Electrical Metrology Division. In 1992, he founded the Applied Precision Ltd., Bratislava, where he is currently a Scientific and Corporate Manager.